Electromagnetic calorimeters based on the scintillating lead tungstate crystals for experiments at Jefferson Lab ☆

A.Asaturyan[a], F.Barbosa[c], V.Berdnikov[b], J.Crafts[g], H.Egiyan[c], L.Gan[f], A.Gasparian[g], K.Harding[c], T.Horn[b], V.Kakoyan[a], H.Mkrtchyan[a], Z.Papandreou[e], V. Popov[c], S.Taylor[c], N.Sandoval[c], A.Somov[c,*], S.Somov[d], A. Smith[h], C. Stanislav[c], H. Voskanyan[a], T. Whitlatch[c], S. Worthington[c]

[a]*A. I. Alikhanian National Science Laboratory (Yerevan Physics Institute), 0036 Yerevan, Armenia*
[b]*Catholic University of America, Washington, DC 20064, USA*
[c]*Thomas Jefferson National Accelerator Facility, Newport News, VA 23606, USA*
[d]*National Research Nuclear University MEPhI, Moscow, Russia*
[e]*University of Regina, Regina, Saskatchewan, Canada S4S 0A2*
[f]*University of North Carolina at Wilmington, Wilmington, NC 28403, USA*
[g]*North Carolina A&T State University, Greensboro, NC 27411, USA*
[h]*Duke University, Durham, North Carolina 27708, USA*

Abstract

A new electromagnetic calorimeter consisting of 140 lead tungstate (PbWO$_4$) scintillating crystals was constructed for the PrimEx η experiment at Jefferson lab. The calorimeter was integrated to the DAQ and trigger systems of the GlueX detector and used in the experiment to reconstruct Compton events. The experiment started collecting data in the Spring of 2019 and acquired about 30% of the required statistics. The calorimeter is a large-scale prototype for the two detectors, which are currently under construction at Jefferson Lab using similar crystals: the Neutral Particle Spectrometer (NPS) and the lead tungstate insert of the forward calorimeter (FCAL) of the GlueX detector. The article presents the design and performance of the Compton calorimeter and describes the FCAL and NPS projects.

Keywords: Electromagnetic calorimeter, Lead tungstate scintillator

1. Introduction

Electromagnetic calorimeters based on the PbWO$_4$ scintillating crystals have a widespread application in experiments in different accelerator facilities such as CERN, FNAL, GSI, and Jefferson Lab (JLab). Electromagnetic showers produced in heavy lead tungstate PbWO$_4$ scintillator crystals with the radiation length of L_R = 0.89 cm and Molière radius of R_m = 2.19 cm have a compact size and provide good separation of electromagnetic showers and resolution of reconstructed energies.

Two electromagnetic calorimeters are currently under construction in the experimental Hall D and Hall C at Jefferson Lab using 2.05 cm x 2.05 cm x 20 cm PbWO$_4$ scintillating modules. The inner part of the forward lead glass calorimeter of the GlueX detector [1] in Hall D will be upgraded with the high-granularity, high-resolution crystals. This upgrade is required by the physics program with the GlueX detector, specifically the new experiment to study rare decays of η mesons [2]. The size of the insert will tentatively consist of 2496 lead tungstate modules. The neutral-particle spectrometer (NPS) [3] in experimental Hall C is a new calorimeter, that will allow to carry out several experiments to study various physics topics such as the transverse spatial and momentum structure of the nucleon. PbWO$_4$ crystals will form an array of 30x36 modules. Lead tungstate crystals were provided by two vendors: Shanghai Institute of Ceramics (SICCAS) in China and CRYTUR in the Czech Republic. The quality of recently produced PbWO$_4$ scintillators has been studied in detail and is described in Ref. [4]. Crystals of the same type are considered to be used in the electromagnetic calorimeter of the future Electron-Ion Collider.

We built a small-size calorimeter prototype composed of 140 SICCAS crystals, which served as the Compton Calorimeter (CCAL) in the PrimEx η experiment [5] with the GlueX detector in the spring of 2019. The CCAL was subsequently used during a few short GlueX physics runs at high luminosity in order to study rates and operation conditions expected for the FCAL lead tungstate insert. Experience gained during fabrication and operation of the CCAL was critical for finalizing the designs of electromagnetic calorimeters of the FCAL and NPS projects.

We will present the PrimEx η experiment and performance of the CCAL in Section 2 and Section 3. The brief description of the FCAL and NPS projects will be given in Sections 4 and 5.
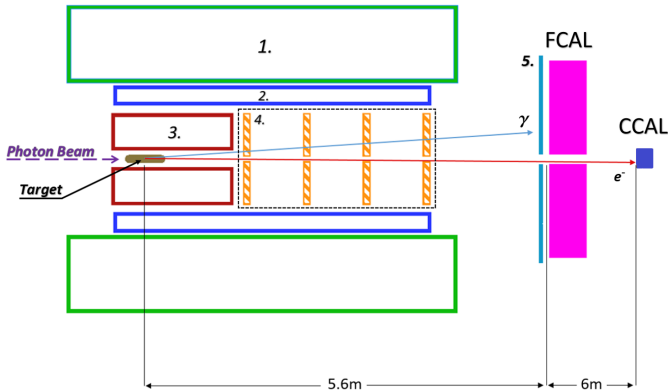
Figure 1: Schematic layout of the GlueX detector (not to scale). Numbers represent the following detector components: solenoid magnet (1), barrel calorimeter (2), central drift chambers (3), forward drift chambers (4), time-of-flight wall (5).
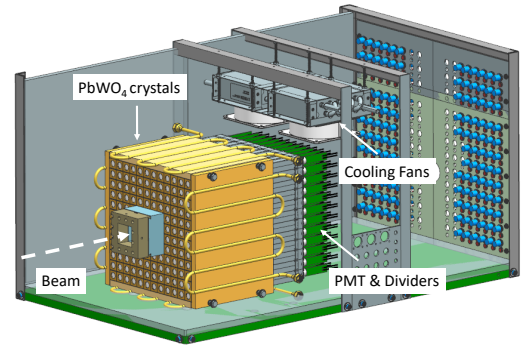
2. PrimEx η experiment with the GlueX detector

The GlueX detector [1] in experimental Hall D was designed to perform experiments using photon beams. Beam photons are produced by electrons provided by the JLab electron accelerator facility, incident on a thin radiator via the bremsstrahlung process. The energy of a beam photon is determined by detecting a scattered bremsstrahlung electron using tagging scintillator detectors with a typical precision of 0.2%.

The physics goal of the PrimEx η experiment is to perform a precision measurement of the $\eta \to \gamma\gamma$ decay width. The measurement will provide an important test of QCD symmetries and is essential for the determination of fundamental properties such as the ratios of the light quark masses and the η-η' mixing angle. The decay width will be extracted from the measurement of the photoproduction cross section of η mesons in the Coulomb field of a nucleus, which is known as the Primakoff effect. η mesons will be reconstructed by detecting two decay photons in the forward calorimeter of the GlueX detector.

The cross section will be normalized using the Compton process, which will also be used to monitor the luminosity and control the detector stability during taking data. Electrons and photon originating from Compton events in the target are produced at small angles typically outside the acceptance of the FCAL. In order to improve reconstruction of particles in the forward direction, we built a small Compton calorimeter consisting of an array of 12 x 12 lead tungstate scintillating crystals (24 cm x 24 cm) and positioned it about 6 m downstream from the FCAL. The CCAL covers the angular range between 0.18° and 0.33°. Schematic view of the GlueX detector and the position of the Compton calorimeter is illustrated in Fig. 1.

The PrimEx η experiment started collecting data in the spring of 2019 and has acquired about 30% of the required statistics. During the experiment, the magnetic field of the solenoid magnet was switched off in order to allow reconstruction of Compton events. The beam photon flux was about four times lower than the nominal GlueX beam conditions. The photon flux was

Figure 2: Schematic layout of the Compton calorimeter.

about $5 \cdot 10^6$ γ/sec in the beam energy range of interest between 9.5 GeV and 11.6 GeV.

3. Compton calorimeter of the PrimEx η experiment

3.1. Calorimeter design

The calorimeter design is shown in Fig. 2. The CCAL is comprises an array of 12 x 12 lead tungstate modules with a 2 x 2 hole in the middle for the photon beam, which are positioned inside a light tight box. A Tungsten absorber is placed in front of the innermost layer closest to the beamline, which is exposed to a high rate of particles predominantly originating from electromagnetic interactions.

The light yield from PbWO$_4$ crystals depends on temperature with the typical temperature coefficient of $2\%/°C$ at room temperature. Maintaining constant temperature is essential for the calorimeter operation. Calorimeter modules are surrounded by four copper plates with built in pipes to circulate the cool liquid and provide temperature stabilization. Foam insulation surrounded the detector box. The temperature was monitored and recorded during the experiment by four thermocouples attached to different points of the PbWO$_4$ module assembly. During the experiment the temperature was maintained at $17 \pm 0.2°C$. The typical heat released by the divider is equivalent to 33 Watts. In order to prevent condensation, the nitrogen purge was applied. Two fans with the water-based cooling system were installed on the top of the crystal assembly to improve nitrogen circulation and heat dissipation from the PMT dividers. The detector was positioned on a movable platform, which provides motion in the vertical and horizontal directions perpendicular to the beam. During detector calibration, each module was moved to the beam.

3.2. Module design

The design of the PbWO$_4$ module is based on the HyCal calorimeter, which was used in several experiments in Jefferson Lab Hall B [6]. An assembled calorimeter module is presented in Fig. 3. The lead tungstate crystal is wrapped with a 60 μm polymer Enhanced Specular Reflector film (ESR) manufactured by 3M^{TM}, which allows 98.5% reflectivity across the
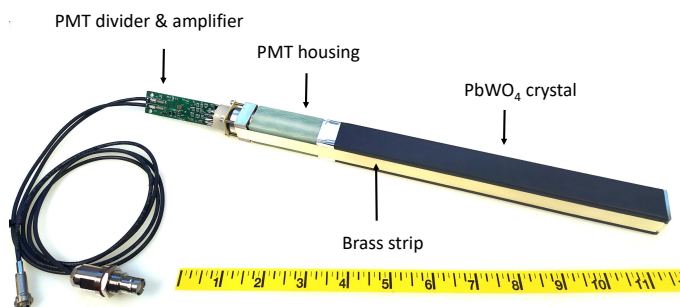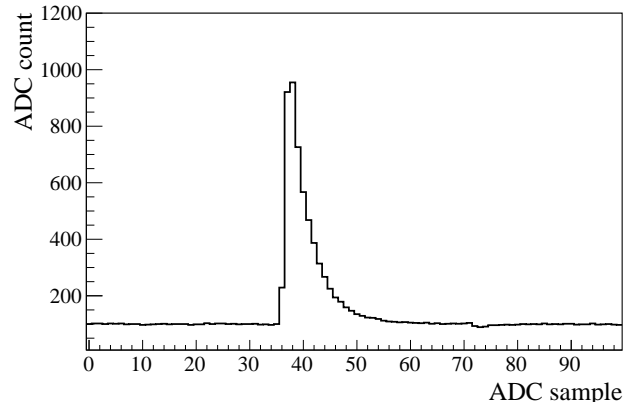
2

Figure 3: Calorimeter module.

Figure 4: A typical flash ADC signal pulse obtained from a PbWO$_4$ module.

visible spectrum. In order to improve optical isolation of each module from its neighbors, each crystal was wrapped with a layer of 25 μm thick Tedlar. The PMT is locates inside a G-10 fiberglass housing at the rear end of the crystal. Two flanges are positioned at the crystal and housing ends and are connected together using 25 μm brass straps, which are brazed to the sides of the flanges. Four set screws are applied to the PMT housing flange to generate tension in the straps and hold the assembly together. Light from the crystal is detected using a ten-stage Hamamatsu PMT 4125, which is inserted to the housing and is coupled to the crystal using optical grease. The PMT diameter is 19 mm. The PMT is pushed towards the crystal by using a G-10 retaining plate attached to the back of the PMT and four tension screws applied to the PMT flange. The PMT is instrumented with a high voltage divider and amplifier positioned on the same printed circuit board, which is attached to the PMT socket.

3.3. Electronics

PMT of each calorimeter module was equipped with an active base prototype [7], which was designed for the Neutral Particle Spectrometer in experimental Hall C. The base combines a voltage divider and an amplifier powered by the current flowing through the divider. The active base allows to operate the PMT at smaller voltage and consequently at lower anode current and therefore improves the detector rate capability. Operation of the PMT at smaller anode current is also important for the extension of the photomultiplier tube life. The original Hamamatsu divider for this type of PMT was modified by adding two bipolar transistors on the last two dynodes, which provides gain stabilization at high rate. The active base from the NPS detector has a relatively large amplification of about a factor of 24 due to the large PMT count rate predicted by Monte Carlo simulation. Large amplification was not needed for run conditions of the PrimEx η experiment. However we subsequently used CCAL in GlueX runs at significantly larger luminosity in order to study run conditions of the FCAL lead tungstate insert, where the amplifier will be required. This will be discussed in Section 4.0.3. During the PrimEx run, the CCAL was operated at about 680 V, which produced a divider current of 260 μA. High voltage

for each PMT was supplied by a 24-channel CAEN A7236SN module positioned in a SY4527 mainframe.

Amplified PMT signals were digitized using a twelve-bit 16-channel flash ADCs electronics module operated at a sampling rate of 250 MHz. The ADC was designed at Jefferson Lab [8] and is used for the instrumentation of several sub-detectors of the GlueX detector. The Field-Programmable Gate Array (FPGA) chip inside the ADC module allows to implement various programmable data processing algorithms for the trigger and readout. An example of a flash ADC signal pulse obtained from a calorimeter module is shown in Fig. 4. In this example the ADC is operated in the raw readout mode, where digitized amplitudes are read out for 100 samples, corresponding to the 400 ns read out window. During the PrimEx η experiment, the ADC performed on-board integration of signal pulses, for amplitudes above a threshold of 24 MeV. ADC amplitudes are summed in a time window of 64 ns and reported by the ADC along with other parameters such as the pulse amplitude, pulse time, amplitude of the ADC pedestal, and data processing quality factors. This readout mode allowed to significantly reduce the data size and ADC read out time, and therefore did not induce any dead time in the DAQ.

CCAL flash ADCs are positioned in a VXS (ANSI/VITA 41.0 standard) crate. VXS crates are used to host all readout electronics of the GlueX experiment. In addition to the VME-bus used to read out data from electronics modules, the VXS is instrumented with a high-speed serial bus in order to increase the bandwidth to several Gb/sec and provide an interconnected network between modules. The bus is used to transmit amplitudes digitized by the ADC to trigger electronics modules and include the CCAL to the Level 1 trigger system of the GlueX detector.

3.4. Light Monitoring System

To monitor performance of each calorimeter channel, we designed an LED-based light monitoring system (LMS). The LMS optics includes a blue LED, a spherical lens to correct the conical dispersion of the LED, and a diffusion grating to homogenize the light. Light produced by the LED is incident on
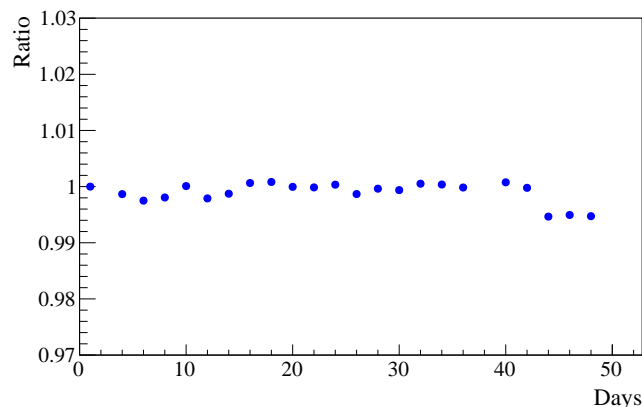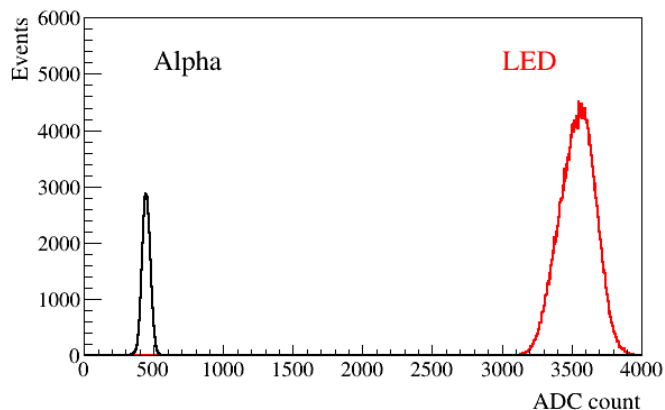
3

Figure 5: Flash ADC signal amplitudes induced by the LED and α-source in the reference PMT.

Figure 6: Ratio of signal ADC amplitudes from the LED pulser to α-source measured by the reference PMT during different run periods of the 48-day long PrimEx η experiment. The ratio is normalized to data in the beginning of the run.

a bundle of plastic optical fibers (Edmund Optics) with a core diameter of 250 μm. Each fiber distributes light to an individual calorimeter module. On the crystal end, the fiber is attached to the module using a small acrylic cap glued to the crystal with a hole drilled through each cap to hold the fiber inside.

To monitor stability of the LED, we used two reference Hamamatsu 4125 PMTs, the same type as in the CCAL detector. Each PMT receives light from two sources: a single fiber from the LED and a YAP:Ce pulser unit, both glued to the PMT face. The pulser unit consists of a 0.15 mm thick YAP:Ce scintillation crystal with a diameter of 3 mm spot activated by an ^{241}Am α source. The α source is used to monitor stability of the LED. The PMT was read out using a flash ADC. The high voltage on each reference PMT was adjusted in such a way to make signals from both the LED and α source fit within the flash ADC range of 4096 counts, as shown in Fig. 5. Each LED was driven by a CAEN 1495 module, which allowed to generate LED pulses with a programmable rate. The LMS was integrated to the GlueX trigger system and provided a special trigger type during data taking. The LMS was extensively used during the detector commissioning and injected light to the CCAL detector with a typical frequency of 100 Hz continuously during the PrimEx η experiment. This LED rate is similar to the trigger rate of events generated by the reference α source.

Most LMS components were positioned inside the temperature-stabilized detector box. The stability of the LED system measured using the reference PMTs during the entire PrimEx run was better than 1%. The ratio of signal ADC amplitudes from the LED pulser to the α alpha source obtained during different run periods of the 48-day long PrimEx η experiment is presented in Fig. 6. The ratio is normalized to the data in the beginning of the experiment. Stability of most CCAL modules observed using the LMS during the experiment was better than 6%. We did not apply any PMT gain adjustments during the experiment.

3.5. Calibration

The initial energy calibration of the CCAL was performed by moving each calorimeter module to the photon beam during special low-intensity calibration runs. The maximum rate in the module for a threshold of 15 MeV did not exceed 200 kHz. The energy of each beam photon was determined by detecting a bremsstrahlung electron using the GlueX tagging detectors as described in Section 2. The tagging detectors cover the photon energy range between 2.9 GeV and 11.4 GeV and provide a relative energy resolution of about 0.2%. The spot size of the collimated photon beam had a diameter of about 6 mm.

In the beginning of the calibration run, we performed adjustment of the PMT high voltage for each module in order to equalize signal pulse amplitudes induced by 10 GeV beam photons. The amplitude was set 3200 ADC counts. An example of flash ADC signal amplitudes in the calorimeter module as a function of the beam energy is presented in Fig. 7. The calibration of each module was refined by reconstructing showers in the calorimeter and constraining the reconstructed energy to the known beam energy.

In calibration runs, we estimated the non-uniformity of 140 CCAL modules by measuring the relative energy resolution for each individual module exposed to the beam. The energy resolution obtained for 6 GeV photons is presented in Fig. 8. The distribution is fit to a Gaussian function. The spread of the distribution is found to be smaller than 5%.

During calibration, we observed some non-linear performance of the PMT active base, with the large amplification factor of 24, on the level of a few percents, which impacted both the pulse peak and pulse integral. The base performance became linear when the amplifier gain was reduced. The CCAL electronics is being currently adjusted; modified active bases will be installed before the new PrimEx η run in 2021. We subsequently replaced the original front end electronics for an array of 3x3 CCAL modules with modified bases where the amplifier was bypassed and measured the energy resolution for different beam energies. An example of the energy deposited by 10 GeV photons incident on the center of the middle module is shown in Fig. 9. The distribution was fit to a Crystal Ball function, which was named after the Crystal Ball collaboration and was
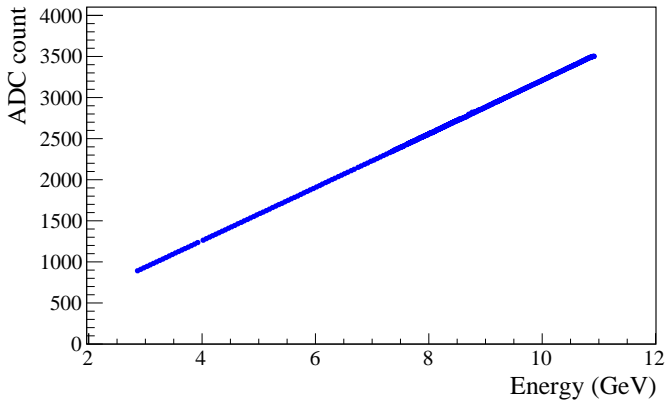
Figure 7: ADC signal pulse amplitude in the CCAL module as a function of the beam energy.
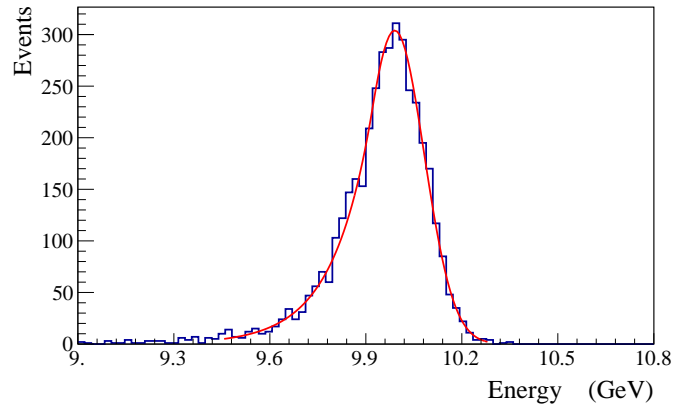

Figure 9: Energy distribution deposited by 10 GeV beam photons. The spectrum is fit to a Crystal Ball function.
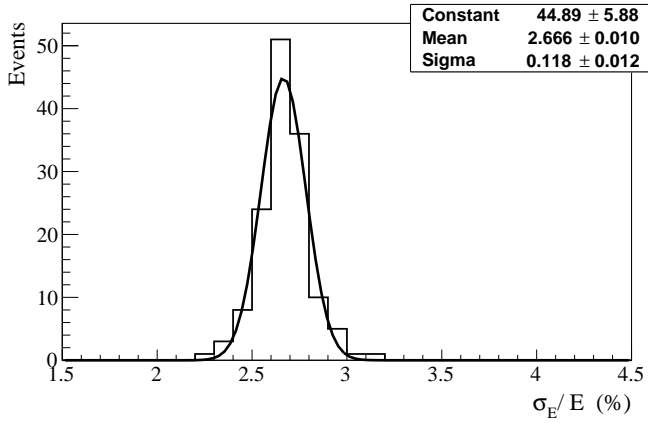

Figure 8: Relative energy resolution of 140 CCAL modules for 6 GeV beam photons.
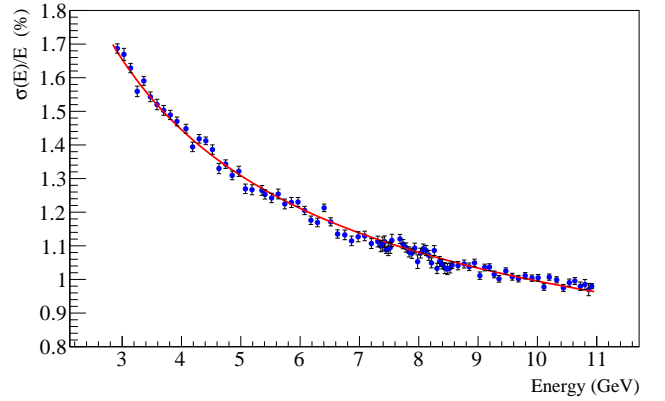

Figure 10: Energy resolution as a function of the photon energy.

implemented in the ROOT data analysis framework [9]. The energy resolution as a function of the beam energy is shown in Fig. 10. The resolution was fit to the following function:

$$\frac{\sigma_E}{E} = \frac{S}{\sqrt{E}} \oplus \frac{N}{E} \oplus C, \quad (1)$$

where S represents the stochastic term, N the noise and C the constant term. E is the beam energy in GeV, and the symbol $\oplus$ indicates a quadratic sum. The fit yields: $S = 2.63 \pm 0.01\%$, $N = 1.07 \pm 0.09\%$, and $C = 0.53 \pm 0.01\%$. The resolution was found to be about 10% better than that measured with the original base with the gain of 24. The energy resolution is consistent with that of the HyCal calorimeter [6], which was instrumented with crystals produced by SICCAS in 2001 and was used in several experiments in Jefferson Lab's experimental Hall B. The HyCal $PbWO_4$ crystals have the same transverse size of 2.05 cm x 2.05 cm, but a smaller length of 18 cm. The CCAL calibration was fine-tuned during the PrimEx run by using showers of reconstructed Compton candidates.

3.6. Performance during the PrimEx run

In the PrimEx η experiment, we reconstruct Compton events produced by beam photons with $E_{beam} > 6$ GeV. This energy range is covered by the pair spectrometer [10], which determines the photon flux needed for cross section measurements. In order to accept Compton events during data taking and to reduce background originating from low-energy electromagnetic and hadronic interactions, the CCAL was integrated to the Level 1 trigger system of the GlueX detector. The physics trigger was based on the total energy deposited in the forward and Compton calorimeters. The GlueX trigger is implemented on special-purpose programmable electronics modules with FPGA chips. The trigger architecture is described in Ref. [11]. The trigger rate as a function of the energy threshold is presented in Fig. 11. We collected data using a relatively small energy threshold of 3 GeV at a trigger rate of about 18 kHz. This rate did not produce any dead time in the DAQ and trigger systems. The trigger rate was reproduced by the detailed Geant detector simulation.

The rate in the CCAL modules during the experiment is presented in Fig. 12. In this plot, the photon beam goes through the
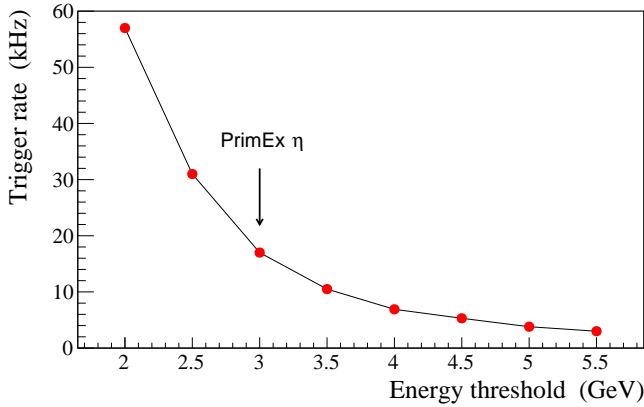
5

Figure 11: Trigger rate as a function of the total energy deposited in the FCAL and CCAL. Arrow indicates the energy threshold used in PrimEx η production runs.
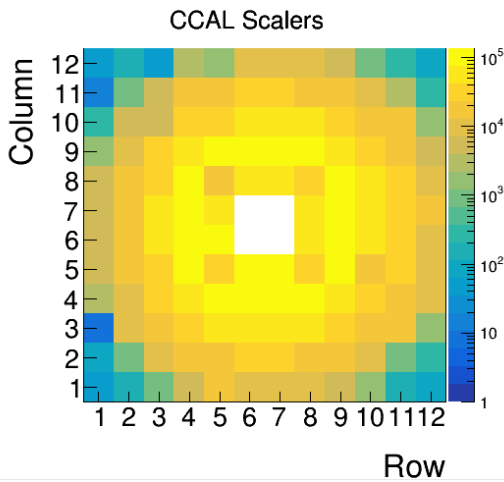

Figure 12: Rates in the CCAL modules during PrimEx η production run. The energy threshold corresponds to 30 MeV. The beam goes through the center of the hole in the middle of the plot.

center of the hole of 2x2 modules in the middle of the detector. The rate is the largest in innermost detector layers closest to the beam line. The maximum trigger rate in the detector module was about 200 kHz for an energy threshold of 30 MeV, which is equivalent to a signal pulse amplitude of 5 mV. Before the experiment, we performed a high-rate performance study of the PMT and electronics using a laser and an LED pulser and did not find any degradation of the PMT gain in run conditions similar to the PrimEx η up to 3-4 MHz [12].

Time resolution of reconstructed showers is an important characteristic of the detector performance. In the experiment, we used timing information provided by calorimeters to identify the accelerator beam bunch where the interaction occurs in the detector and therefore relate showers in the calorimeters with hits in the tagging detector, from the same event. A hit in the tagging detector defines the energy of the beam photon. The time of a hit in the calorimeter module is provided by an algorithm implemented on the programmable FPGA chip of the flash ADC. The algorithm performs a search of the peak of the signal pulse and determines time from the shape of the leading edge of the pulse. The times of all hits constituting the CCAL shower are combined to form shower time by using an energy-weighted sum. The time difference between beam photon candidates and CCAL showers originating from Compton events is presented in Fig. 13. The main peak on this plot corresponds to beam photons and CCAL clusters produced in the same accelerator bunch. Satellites peaks separated by the beam bunch period of about 4 ns represent accidental beam photons, not associated with the detector time. The time resolution of CCAL showers is improved with the increase of the shower energy and was measured to be about 330 ps and 140 ps for 1 GeV and 9 GeV showers, respectively. In the PrimEx experiment, CCAL allowed to clearly separate beam photons originating from different beam bunches.

An electron and photon produced in the Compton scattering process were detected by reconstructing two showers, one in the FCAL and another one in CCAL. The event topology of the reaction is such that the more energetic electron predominantly goes into the Compton calorimeter, while the photon is sent to the FCAL. Reconstruction of electromagnetic showers in the FCAL is performed using an algorithm described in Ref. [13], which is a part of the standard GlueX reconstruction software. For the CCAL, we implemented an algorithm originally developed for the GAMS spectrometer [14], which was later adopted for the HyCal [6] in JLab's experimental Hall B. The algorithm provides a good separation of overlapping showers in the calorimeter by using profiles of electromagnetic showers. The elasticity distribution, defined as the reconstructed energy in the event minus the beam energy, for Compton candidates produced by beam photons in the energy range between 6 GeV and 7 GeV is presented in Fig. 14. The solid line shows the fit of this distribution to the sum of a Gaussian and a second order polynomial functions. The energy resolution of reconstructed Compton candidates is about 150 MeV. In this plot, we subtracted background originating from multiple beam photon candidates in the event due to accidental hits in the GlueX tagging detectors. The background was measured using off-time interactions and amounted to about 15%. The relatively small background, on the level of 10%, produced by interactions of beam photons with the beamline material downstream the GlueX target was measured using empty-target runs and was excluded from Fig. 14. The CCAL allowed to clearly reconstruct Compton events in the PrimEx η experiment.

4. Upgrade of the GlueX forward calorimeter

The forward calorimeter of the GlueX detector consists of 2800 lead glass modules, with a size of 4 cm x 4 cm x 45 cm, and is positioned about 6 m downstream of the target, as shown in Fig. 1. The FCAL covers a polar angle of photons produced from the target between 1° and 11° and detects showers with energies in the range of 0.1 - 8 GeV. The Cherenkov light produced in the module is detected by FEU-84-3 photomultiplier tubes produced Russia, instrumented with Cockcroft-
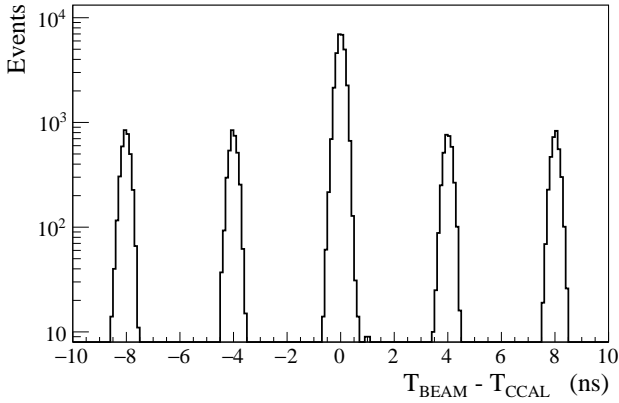
Figure 13: Time difference between beam photons and reconstructed CCAL showers for Compton candidates. Peaks are separated by the beam bunch period of 4 ns.
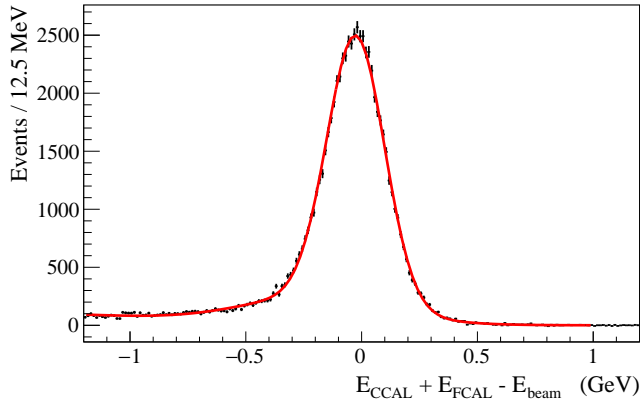

Figure 14: Elasticity distribution of reconstructed Compton candidates.
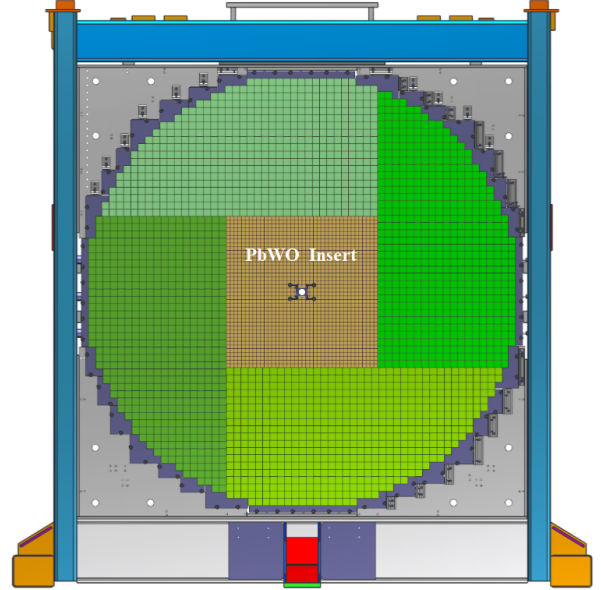

Figure 15: FCAL frame with calorimeter modules installed: $PbWO_4$ crystals (brown area), lead glass blocks (green). Photon beam goes in the hole in the middle of the calorimeter.

Walton bases [15]. The typical energy resolution of the FCAL is $\sigma_E/E = 6.2\%/\sqrt{E} \oplus 4.7\%$.

The future physics program with the GlueX detector in experimental Hall D will require an upgrade of the inner part of the forward calorimeter with high-granularity, high-resolution PbW0$_4$ crystals. The lead tungstate insert will improve the separation of clusters in the forward direction and the energy resolution of reconstructed photons by about a factor of two. Lead tungstate crystals possess better radiation hardness compared to lead glass, which is important for the long term operation of the detector at high luminosity. We propose to build a 1 m x 1 m insert, which will require about 2496 modules. Similar to the CCAL, the insert will have a beam hole of 2 x 2 modules and a Tungsten absorber used to cover the detector layer closest to the beamline. A schematic view of the FCAL frame with the installed lead tungstate insert is presented in Fig. 15. Due to the different size of the lead glass bars and lead tungstate crystals, the lead glass modules stacked around the PbW0$_4$ insert will form four regions with a relative offset between modules; those regions are shown in green color in this plot.

The PbW0$_4$ module design of the FCAL insert will essen-

tially be the same as for the CCAL, except for some small modifications needed to handle the magnetic field present in the FCAL region. The PMT housing made of the G-10 fiberglass material will be replaced by iron housing in order to reduce the magnetic field. The housing length will be increased to extended the magnetic shield beyond the PMT photo cathode. An acrylic optical light guide will be inserted inside the PMT housing to couple the crystal and PMT.

The upgraded FCAL will be operated in GlueX experiments using a 30 cm long liquid hydrogen target at the designed photon flux of $5 \cdot 10^7$ γ/sec in the energy range between 8 GeV and 9 GeV. The designed luminosity is significantly larger than that used in the PrimEx η experiment and was achieved after the PrimEx run in the fall of 2019. In order to finalize the design of the PMT electronics, it is important to understand detector rates in the FCAL insert, especially in layers close to the beamline. We used CCAL during high-intensity GlueX runs to study run conditions for the FCAL insert.

4.0.1. PMT magnetic shield

The longitudinal (directed along the beamline) and transverse (directed perpendicular to the axis of of the beamline) components of the magnetic field produced by the GlueX solenoid magnet in the FCAL PbWO$_4$ insert area vary between 40 - 50 Gauss and 0 - 8 Gauss, respectively. The longitudinal filed is the largest on the beamline, where the transverse component is practically absent. We studied the PMT magnetic shielding using a prototype consisting of an array of 3x3 PMT iron housings made of AISI 1020 steel, which was positioned in the middle of Helmholtz coils. Each housing had a size of 20.6 mm x 20.6 mm x 100 mm with a 19.9 mm round hole in the middle for the PMT. This corresponds to the realistic size of the magnetic
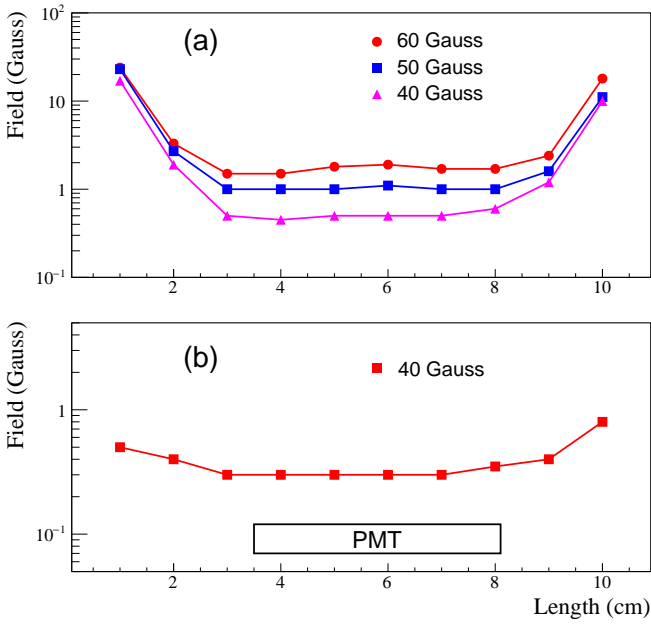
Figure 16: Magnetic field distribution inside the PMT shield housing as a function of the distance from the housing face. Plot (a) corresponds to the longitudinal field and plot (b) corresponds to the transverse field. Markers denote different field values produced by the Helmholtz coils.
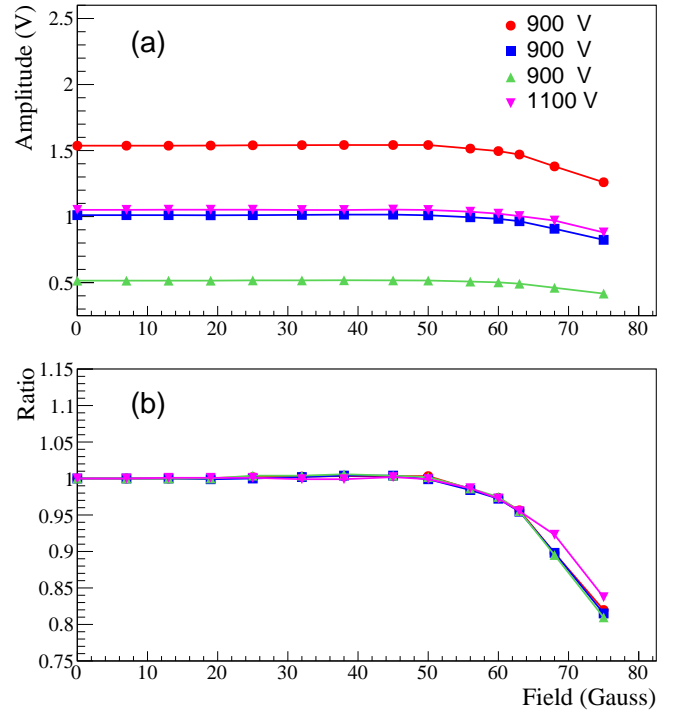

Figure 17: Signal amplitudes of shielded PMT induced by an LED as a function of the magnetic field (a). Amplitudes, normalized to measurements without magnetic field (b). PMT response was measured for different intensities of light pulse and HV settings as shown by different polymarkers.

shield that will be used in the calorimeter module assembly. Inside the housing we inserted two layers of μ-metal Co-Netic cylinders, with thicknesses of 350 μm and 50 μm, separated from each other by a Kapton film. The thickest cylinder was spot welded and annealed.

The Helmholtz coils had a diameter of about 1 m and can generate a uniform magnetic field with variable strength below 100 Gauss. A Hall probe was inserted into the central module of the prototype to measure the magnetic field at different Z-positions along the length of the cylinder. The field was measured for two different orientations of the prototype with respect to the magnetic field: field oriented along the PMT (longitudinal, B_z) and perpendicular to the PMT housing (transverse, B_x). Field measurements are presented in Fig. 16. The PMT shield significantly reduce both the longitudinal and transverse fields to the level of $B_z \sim 1$ Gauss and $B_x \ll 1$ Gauss. The transverse field, which is well shielded, is more critical for the PMT operation, as it is directed perpendicular to the electron trajectory inside the photo tube and deflects electrons, resulting in the degradation of the photon detector efficiency and gain. The field reaches a plateau at $Z = 3$ cm from the face of the housing. We will use 3.5 cm long acrylic light guides, in order to place the most sensitive to the magnetic field area of the PMT between the photocathode and the last dynode (4.6 cm long) in the region with the smallest magnetic field, as shown in Fig. 16.

We studied performance of the shielded PMT in the magnetic field using an LED pulser. A blue LED with a light diffuser was placed about 20 cm from the PMT housing prototype and was aligned with the middle module. The PMT response was measured for different pulse amplitudes and operational high volt-

age. In order to study the contributions from longitudinal and transverse field components we rotated the prototype by different angles. Signal amplitudes as a function of the magnetic field measured in the prototype tilted by about 10 degrees are presented on the left plot of Fig. 17. Amplitudes, normalized to measurements without magnetic field, are shown on the bottom plot. The relative degradation of the signal amplitude for the maximum field in the FCAL insert region of B = 50 Gauss (B_z = 49 Gauss and B_x = 8.6 Gauss) was measured to be less than 1%.

4.0.2. Light guide studies

Studies of the magnetic shielding demonstrated that the PMT has to be positioned inside the iron housing and Co-Netic μ-metal cylinder at the distance of at least 3 cm from the face of the PbWO$_4$ crystal. In the FCAL insert module, we decided to use a 3.5 cm long acrylic cylindrical light guide with a diameter of 18.5 mm between the PMT and the crystal. The light guide is wrapped with reflective ESR foil. The light guide is attached to the PMT with Dymax 3094 UV curing glue. Optical coupling to the crystal is provided by a "silicon cookie": a 1 mm thick transparent rubber cylinder made of the room temperature vulcanized silicon compound, RTV615. This type of material has a widespread application in photodetectors and simplifies the module design. The silicon cookie is not glued to the light guide and the crystal, so the module can be easily disassembles
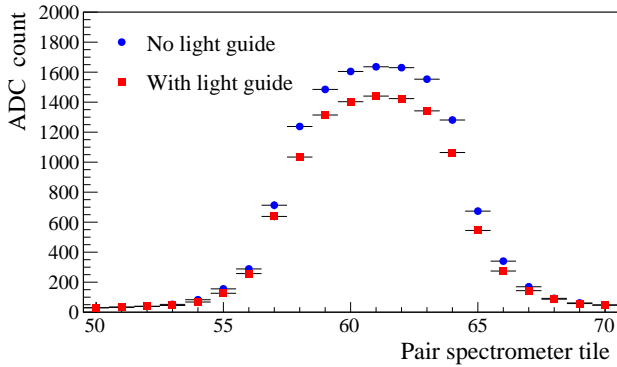
Figure 18: ADC amplitudes of the calorimeter module as a function of the pair spectrometer tile for two configurations: PMT directly coupled to the PbWO$_4$ crystal (circles), PMT coupled to the module using an optical light guide (boxes).
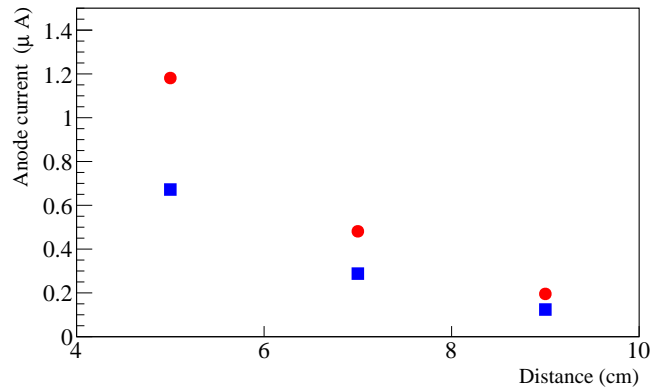

Figure 19: Typical PMT anode current of CCAL modules positioned at different distances from the beamline. Circles correspond to the nominal GlueX luminosity, boxes correspond to 60% of the nominal luminosity.

if PMT needs to be replaced.

We compared light losses of the FCAL insert module instrumented with the light guide with the CCAL module, where PMT is coupled directly to the crystal using an optical grease. Light collection was measured using electrons provided by the Hall D pair spectrometer (PS) [10]. The PS is used to measure the flux of beam photons delivered to the experimental hall by detecting electromagnetic electron-positron pairs produced by the photons in a thin converter inserted to the beam. Leptons from the pair are deflected in a dipole magnet and detected using two scintillator detectors placed in the electron and positron arms of the spectrometer. Each detector consists of 145 tiles, which cover the energy range of leptons between 3 GeV and 6 GeV.

We first positioned the CCAL module behind the PS and measured ADC amplitudes of signal pulses induced by electrons with the energy of about 4 GeV. The module was subsequently modified by adding the light guide to the same PMT and crystal and was placed to the same spot of the PS test setup. Results of the measurements are presented Fig. 18. On this plot the ADC amplitude of the calorimeter module is presented as a function of the PS tile for the two module configurations with and without the light guide. The light guide results in a relatively small loss of light of about 15% compared with the CCAL module. We note that wrapping light guide with the reflective material is important. Losses in unwrapped light guide constitute about 35%. We repeated light collection measurements using two more modules and obtained consistent results.

4.0.3. Detector rate

The PMT anode current is one of the critical characteristics that have to be considered during the design of the PMT divider. Typically the anode current should be on the level of a few micro amperes and significantly smaller than the divider current in order to provide stable performance of the PMT base and prevent the long-term degradation of the PMT. The anode current was measured using a special random trigger, which was used to read out flash ADC raw data for each CCAL channel in a time window of 400 ns. The window size corresponds to 100 flash ADC samples. The average ADC voltage in the readout window was determined by summing up amplitudes and normalizing them to the window size. The voltage measured by the ADC is produced by the current going through a ~ 50 Ω termination resistor. The anode current can be estimated as

$$I = \frac{\bar{A}}{R} \cdot \frac{1}{G}, \qquad (2)$$

where $\bar{A}$ is the average ADC amplitude in the readout window in units of Volts, R is the termination resistor, and G is the amplifier gain of 24. The typical anode current measured in CCAL modules situated at different distances from the beam line is presented in Fig. 19. Modules from the first CCAL layer closest to the beamline and the outer most layer were not used in the analysis. These modules were covered by a Tungsten absorber and obscured by the FCAL. The rate in the detector is dominated by the forward-directed electromagnetic background. The anode current is the largest in the innermost layer of the detector closest to the beam line and amounts to about 1.4 μA. This current can be compared to the PMT divider current of 300 μA. The CCAL measurements can be used to estimate anode current in the FCAL lead tungstate insert. The largest PMT current in the PbWO$_4$ module closest to the beam line is conservatively estimated to be about 20 μA for a PMT base operated at 1 kV, and assuming that no amplifier is used. The detector rate drops rapidly with the increase of the radial distance from the beamline. We are considering to instrument PMTs in a few inner layers with an amplifier with a gain of 5 and to omit the amplifier on other modules.

5. Neutral Particle Spectrometer

The neutral-particle spectrometer offers unique scientific capabilities to study the transverse spatial and momentum structure of the nucleon in the Jefferson Lab experimental Hall C. Much progress in imaging nucleon structure can be made

with electron-scattering reactions, yet experiments with high-energy photons play a unique complementary role. The small scattering probabilities of exclusive reactions demand high-intensity photon beams. Understanding strengthened by imaging longitudinally-polarized and transversely-polarized nucleons. Five experiments have been currently approved using the NPS. The experiments will use a high-intensity beam of electrons, with a typical lumonisity of $\sim 10^{38}$ cm^{-2}s^{-1} as well as a secondary beam of photons incident on a liquid hydrogen target.

Similar to the FCAL insert in experimental Hall D, the NPS will be built from the same type of crystals, and instrumented with the same PMTs and readout electronics. The NPS consists of 1080 $PbWO_4$ crystals, which form an array of 30x36 modules. The detector is positioned on a movable platforms in a temperature controlled frame designed by INPN Orsay. In different experiments, the detector will be placed at different angles between 5.5 and 60 degrees with respect to the Hall C beamline. A sweep magnet will be installed in front of the spectrometer in order to reduce background of charged particle tracks originating from the target. The integrated field of the magnet varies between 0.3 Tm and 0.6 Tm depending on the distance of the NPS detector from the beamline. The maximum fringe field originating from the magnet in the detector region is 200 Gauss.

$PbWO_4$ crystals produced by CRYTUR are expected to have slightly better radiation hardness compared to the SICCAS crystals [4]. The CRYTUR crystals will be installed in the region close to the beamline, where the radiation level is the highest, whereas the SICCAS crystals will be placed at the edges of the detector further away from the beam. Each crystal will be wrapped with the reflective ESR foil. The crystal's support structure consists of horizontal and vertical layers of 0.5 mm thick carbon plates. Each crystal is positioned inside a cell surrounded by the carbon plates. Hamamatsu R4125 PMT is situated inside a round μ-metal housing with an out diameter of 19.6 mm and is attached to the back side of each module. In order to provide additional magnetic field shielding, 0.5 mm thick μ-metal plates are used around the PMT housing. The initial magnetic field is reduced by surrounding the NPS frame, except the face and the back of the detector, by a 10 mm thick soft iron shield box.

The design of the PMT base will be adjusted according to run conditions of experiments with the NPS. The gain of the amplifier will be determined according to rates expected in the detector, which are currently sumulated using Geant detector simulation. Signal pulses from the PMT are digitized using flash ADCs hosted in VXS crates. High voltage for PMTs is supplied by a 36-channel CAEN 7030N module installed in a SY4527 crate. Energy deposition in the calorimeter, will be used in the trigger system of the experiments. Integration of the detector to the trigger will be performed by means of the trigger electronics modules designed at Jefferson Lab. A blue LED is distributed to each calorimeter module through a quartz optical fiber, glued to the crystal from the PMT side. The LED system will be used for calibration and allow to cure crystals whose performance is degraded due to radiation. The cluster reconstruction software of the NPS is currently under development. It will adopt the already existing clustering algorithm of the DVCS experiment in experimental Hall A [reference needed].

6. Summary

We described the design and performance of the Compton calorimeter, which was constructed using 140 lead tungstate $PbWO_4$ crystals recently produced by SICCAS. The calorimeter was successfully used in the PrimEx η experiment in spring of 2019 for reconstruction of Compton events. The CCAL served as a prototype for two large-scale electromagnetic calorimeters, designed to use $PbWO_4$ crystals of the same size: the lead tungstate insert of the forward calorimeter of the GlueX detector and the neutral particle spectrometer. Experience gained during construction and operation of the CCAL provided important information for finalizing the design of these electromagnetic calorimeters. The design of the NPS and FCAL lead tungstate insert was presented.

7. Acknowledgments

References

[1] S. Adhikari, *et al.*, Nucl. Instrum. Meth. A **987**, 164807 (2021).

[2] JLab Experiment E12-12-002A, (2014) `https://www.jlab.org/exp_prog/proposals/14/PR12-14-004.pdf`.

[3] T. Horn, J. Phys. Conf. Ser. **587** (2015) no.1, 012048.

[4] T. Horn, *et al.*, Nucl. Instrum. Meth. A **956**, 163375 (2020).

[5] JLab Experiment E12-10-011, (2009) `https://www.jlab.org/exp_prog/proposals/10/PR12-10-011.pdf`.
http://www.wiener-d.com/sc/powered-crates/vxs/

[6] M. Kubantsev *et al.*, AIP Conf. Proc. **867**, no.1, 51-58 (2006). A. Gasparian, Proceedings of the 11th International Conference on Calorimetry in High-Energy Physics, 109-115 (2004).

[7] V. Popov and H. Mkrtchyan *et al.*, Proceedings of the IEEE conference, California, 2012.

[8] F. Barbosa *et al.*, Proceedings of IEEE Nuclear Science Symposium, Hawaii, USA (2007).

[9] R. Brun and F. Rademakers, Nucl. Instrum. Meth. A **389** (1997), 81-86.

[10] F. Barbosa, *et al.*, Nucl. Instrum. Meth. A **795**, 376-380 (2015).

[11] A. Somov, AIP Conf. Proc. **1560**, no.1, 700-702 (2013).

[12] F. Barbosa, *et al.*, "Characterization of the NPS and CCAL readout," GlueX-doc-3272, Jefferson Lab, (2017), `https://halldweb.jlab.org/doc-public/DocDB/ShowDocument?docid=3272`.

[13] R. Jones, *et al.*, Nucl. Instrum. Meth. A566, 366374, (2006).

[14] A. Lednev, Preprint IHEP 93-153, Protvino (1993). F. Binon, *et al.*, Nucl. Instrum. Meth. A **248**, (1986).

[15] A. Brunner, et al., *et al.*, Nucl.Instrum. Meth. A414 (1998).